antiferromagnetic (positive value) and very weak, as expected for an exchange interaction via the six C−H···Cl and the Cl···Cl pathways. A value of $J \approx 0.1$ K was also obtained from d.c. susceptibility measurements in the 1 to 8 K range.

The above results demonstrate that even weak exchange interactions can have a large influence of the quantum properties of SMMs. From one viewpoint, each half of the $[Mn4]_2$ dimer acts as a field bias on its neighbour, shifting the tunnel resonances to new positions relative to isolated Mn4 molecules. In particular, these single Mn4 molecules show a strong QTM step at zero field in the hysteresis loop[23], a feature absent for $[Mn4]_2$ (Fig. 2) because this would be a double quantum transition with a very low probability of occurrence. The absence of tunnelling at zero field is important if SMMs are to be used for information storage, and the option is still retained to switch on tunnelling, if and when required, by application of a field. Thus, future studies will investigate this double transition at zero field in $[Mn4]_2$, and the corresponding multiple quantum transition in higher supramolecular aggregates of SMMs, and determine their exact probability of occurrence and to what extent this can be controlled by the degree of aggregation, variation of exchange coupling strength and similar modifications. From another viewpoint, $[Mn4]_2$ represents an example of quantum tunnelling within a monodisperse antiferromagnetically coupled particle with no uncompensated spin (that is, $S = 0$) in the ground state. It may also prove possible to study its $(9/2, -9/2)$ to $(-9/2, 9/2)$ tunnelling transition. This would be analogous to the transition in antiferromagnets, in which tunnelling is predicted[27] to be more pronounced than in ferromagnets. Such a study for ferritin suffered from the practical impossibility of having all molecules in the sample be the same size, and possess completely compensated spins[28−30]. Finally, the absence of a level crossing at zero field also makes $[Mn4]_2$ a very interesting candidate as a qubit for quantum computing[8], because its ground state is the entangled combination of the $(9/2, -9/2)$ and $(-9/2, 9/2)$ states; the coupling of this $S = 0$ system to environmental degrees of freedom should be small, which means decoherence effects should also be small.

In future work, we shall use the Landau−Zener method[20] to determine the tunnel splitting in $[Mn4]_2$, and apply a transverse field to probe its exact influence on QTM rates (we have already confirmed that a transverse field increases the tunnelling rate, as expected for QTM). The identification of both an antiferromagnetic coupling and an exchange-bias effect in $[Mn4]_2$ demonstrates the feasibility of employing supramolecular chemistry to modulate the quantum physics of SMMs, providing a realistic method for fine-tuning the properties of these molecular nanoscale materials. This brings closer their use in devices.

1. Sessoli, R. *et al.* High-spin molecules: $[Mn_{12}O_{12}(O_2CR)_{16}(H_2O)_4]$. *J. Am. Chem. Soc.* **115,** 1804–1816 (1993).
2. Sessoli, R., Gatteschi, D., Caneschi, A. & Novak, M. A. Magnetic bistability in a metal-ion cluster. *Nature* **365,** 141–143 (1993).
3. Christou, G., Gatteschi, D., Hendrickson, D. N. & Sessoli, R. Single-molecule magnets. *MRS Bull.*. **25,** 66–71 (2000).
4. Aubin, S. M. J. *et al.* Distorted $Mn^{IV}Mn^{III}_3$ cubane complexes as single-molecule magnets. *J. Am. Chem. Soc.* **118,** 7746–7754 (1996).
5. Friedman, J. R., Sarachik, M. P., Tejada, J. & Ziolo, R. Macroscopic measurement of resonant magnetization tunnelling in high-spin molecules. *Phys. Rev. Lett.* **76,** 3830–3833 (1996).
6. Thomas, L. *et al.* Macroscopic quantum tunneling of magnetization in a single crystal of nanomagnets. *Nature* **383,** 145–147 (1996).
7. Wernsdorfer, W. & Sessoli, R. Quantum phase interference and parity effects in magnetic molecular clusters. *Science* **284,** 133–135 (1999).
8. Leuenberger, M. N. & Loss, D. Quantum computing in molecular magnets. *Nature* **410,** 789–793 (2001).
9. Hendrickson, D. N. *et al.* Photosynthetic water oxidation center: spin frustration in distorted cubane $Mn^{IV}Mn^{III}_3$ model complexes. *J. Am. Chem. Soc.* **114,** 2455–2471 (1992).
10. Desiraju, G. R. The C−H···O hydrogen bond: structural implications and supramolecular design. *Acc. Chem. Res.* **29,** 441–449 (1996).
11. Freytag, M. & Jones, P. G. Hydrogen bonds C−H···Cl as a structure-determining factor in the gold(I) complex bis(3-bromopyridine)gold(I) dichloroaurate(I). *Chem. Commun.* 277–278 (2000).
12. Aullón, G., Bellamy, D., Brammer, L., Bruton, E. A. & Orpen, A. G. Metal-bound chlorine often accepts hydrogen bonds. *Chem. Commun.* 653–654 (1998).
13. Raymo, F. M., Bartberger, M. D., Houk, K. N. & Stoddart, J. F. The magnitude of [C−H···O] hydrogen bonding in molecular and supramolecular assemblies. *J. Am. Chem. Soc.* **123,** 9264–9267 (2001).
14. Jeffrey, G. A. & Saenger, W. *Hydrogen Bonding in Biological Structures* (Springer, Berlin, 1991).
15. Desiraju, G. R. *Crystal Engineering: the Design of Organic Solids* (Elsevier, Amsterdam, 1989).
16. Jones, P. G. & Ahrens, B. Bis(diphenylphosphino)methane and related ligands as hydrogen bond donors. *Chem. Commun.* 2307–2308 (1998).
17. Xu, C. *et al.* Synthesis, molecular structures and fluxional behavior of dppm-bridged complexes of platinum(II) with linear gold(I), trigonal silver(I), or tetrahedral mercury(II) centers. *Organometallics* **15,** 3972–3979 (1996).
18. Wemple, M. W., Tsai, H.-L., Folting, K., Hendrickson, D. N. & Christou, G. Distorted cubane $[Mn_4O_3Cl]^{6+}$ complexes with arenecarboxylate ligation: crystallographic, magnetochemical and spectroscopic characterization. *Inorg. Chem.* **32,** 2025–2031 (1993).
19. Carlin, R. L. *Magnetochemistry* (Springer, Berlin, 1986).
20. Wernsdorfer, W. Classical and quantum magnetization reversal studies in nanometer-sized particles and clusters. *Adv. Chem. Phys.* **118,** 99–190 (2001).
21. Sangregorio, C. *et al.* Quantum tunnelling of the magnetization in an iron cluster nanomagnet. *Phys. Rev. Lett.* **78,** 4645–4648 (1997).
22. Aubin, S. M. J. *et al.* Half-integer-spin, single-molecule magnet exhibiting resonant magnetization tunnelling. *J. Am. Chem. Soc.* **120,** 839–840 (1998).
23. Aubin, S. M. J. *et al.* Resonant magnetization tunnelling in the trigonal pyramidal $Mn^{IV}Mn^{III}_3$ complex $[Mn_4O_3Cl(O_2CMe)_3(dbm)_3]$. *J. Am. Chem. Soc.* **120,** 4991–5004 (1998).
24. Aubin, S. M. J. *et al.* Resonant magnetization tunnelling in the half-integer-spin single-molecular magnet $[PPh_4][Mn_{12}O_{12}(O_2CEt)_{16}(H_2O)_4]$. *Chem. Commun.* 803–804 (1998).
25. Boskovic, C., Pink, M., Huffman, J. C., Hendrickson, D. N. & Christou, G. Single-molecule magnets: ligand-induced core distortion and multiple Jahn−Teller isomerism in $[Mn_{12}O_{12}(OAc)_8(O_2PPh_2)_8(H_2O)_4]$. *J. Am. Chem. Soc.* **123,** 9914–9915 (2001).
26. Andres, H. *et al.* Inelastic neutron scattering and magnetic susceptibilities of the single-molecule magnets $[Mn_4O_3X(OAc)_3(dbm)_3]$ (X = Br, Cl, OAc, and F): variation of the anisotropy along the series. *J. Am. Chem. Soc.* **122,** 12469–12477 (2000).
27. Barbara, B. & Chudnovsky, E. M. Macroscopic quantum tunneling in antiferromagnets. *Phys. Lett. A* **145,** 205–208 (1990).
28. Awschalom, D. D., Smyth, J. F., Grinstein, G., DiVincenzo, D. P. & Loss, D. Macroscopic quantum tunneling in magnetic proteins. *Phys. Rev. Lett.* **68,** 3092–3095 (1992).
29. Gider, S., Awschalom, D. D., Douglas, T., Mann, S. & Chaparala, M. Classical and quantum magnetic phenomena in natural and artificial ferritin proteins. *Science* **268,** 77–80 (1995).
30. Tejada, J. *et al.* Does macroscopic quantum coherence occur in ferritin? *Science* **272,** 424–426 (1996).

Molecular dynamics simulation of the ice nucleation and growth process leading to water freezing

Masakazu Matsumoto, Shinji Saito & Iwao Ohmine

Chemistry Department, Nagoya University, Chikusa-ku, Nagoya, Japan 464-8602

Upon cooling, water freezes to ice. This familiar phase transition occurs widely in nature, yet unlike the freezing of simple liquids[1−3], it has never been successfully simulated on a computer. The difficulty lies with the fact that hydrogen bonding between individual water molecules yields a disordered three-dimensional hydrogen-bond network whose rugged and complex global potential energy surface[4−6] permits a large number of possible network configurations. As a result, it is very challenging to reproduce the freezing of 'real' water into a solid with a unique crystalline structure. For systems with a limited number of possible disordered hydrogen-bond network structures, such as

confined water, it is relatively easy to locate a pathway from a liquid state to a crystalline structure[7–9]. For pure and spatially unconfined water, however, molecular dynamics simulations of freezing are severely hampered by the large number of possible network configurations that exist. Here we present a molecular dynamics trajectory that captures the molecular processes involved in the freezing of pure water. We find that ice nucleation occurs once a sufficient number of relatively long-lived hydrogen bonds develop spontaneously at the same location to form a fairly compact initial nucleus. The initial nucleus then slowly changes shape and size until it reaches a stage that allows rapid expansion, resulting in crystallization of the entire system.

The difficulties associated with simulating the freezing of water resemble those of the protein-folding problem: real proteins fold into a unique native structure from numerous denatured states[10,11], but attempts to simulate this process for large proteins remain, so far, unsuccessful.

Our molecular dynamics (MD) simulation of the water-freezing process involves thermalization of pure water at a high temperature, followed by quenching (at time $t = 0$) to a low temperature, 230 K.
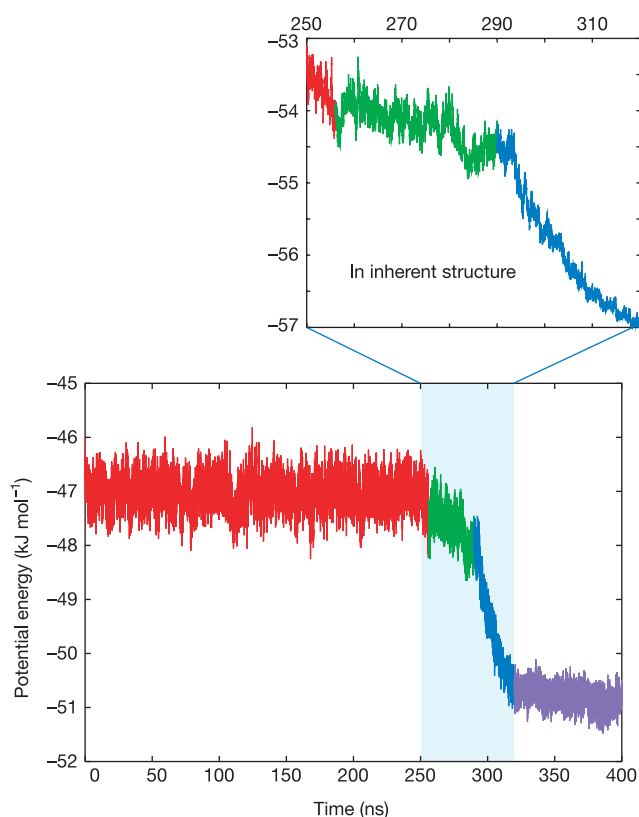

Figure 1 The total potential energies of the instantaneous structures in the trajectory for 512 water molecules after quenching (at $t = 0$ ns) from higher temperature to 230 K. Sufficient thermalization at the high temperature (400 K) is performed before the temperature jump. A constant-temperature and constant-volume molecular dynamics (MD) method is used for a system with 512 water molecules, confined in a cubic box under a periodic boundary condition. The TIP4P water model is used. The inset shows the total potential energies of the inherent structures, corresponding to the instantaneous structures in the trajectory for $t = 250$–320 ns. Inherent structures are calculated by local quenching at 10-ps intervals. Energy is in kJ mol^{-1} and time in ns (10^{-9} s). We note that the freezing process can be divided into four stages: (1) a long quiescent period (indicated by a red line); (2) a slow energy-decreasing period (green line); (3) a fast energy-decreasing period (dark blue line); and (4) a crystallization-completion period (purple line).

The system is then monitored for crystallization for $t > 0$ while keeping the temperature at 230 K. At this temperature, water is in a supercooled state. Because the density of our system (0.96 g cm^{-3}) is slightly lower than that of normal liquid water, the degree of supercooling and hence also the nucleation rate is increased. Nevertheless, many MD trajectory calculations, each longer than 1 µs, are needed to obtain a trajectory that leads to crystallization.

Figure 1 gives the total potential energy as a function of time for one such trajectory in a system of 512 water molecules. The data show that there are four stages in the freezing process: (1) a long quiescent period with relatively constant potential energy ($t = 0$–256 ns); (2) a short period during which the potential energy slowly decreases ($t = 256$–290 ns); (3) a short period during which the potential energy decreases rapidly ($t = 290$–320 ns); and (4) a final period with reduced but relatively constant potential energy and during which the ice structure fully forms ($t > 320$ ns). Water in the quiescent period is in a supercooled liquid state, exhibiting intermittent collective motions and energy fluctuations associated with hydrogen bond rearrangements. The freezing process starts in stage (2). The fact that the system explores the overall relatively flat potential energy landscape for a considerable time (that is, the quiescent period) before entering the fast growing period agrees with the predictions of basic nucleation theory[12–14]. However, the MD simulation also provides a molecular-level illustration of the water freezing process not obtainable from conventional nucleation theory[14].

Figure 2 depicts the hydrogen-bond structure of the system at different times after quenching. In the quiescent period (Fig. 2a), the hydrogen-bond network contains mainly five-, six- and seven-membered rings composed of water molecules held together by hydrogen bonds. Although individual rings are destroyed and reformed continuously, the overall fraction of water molecules contained in the different ring types remains almost unchanged during the quiescent period, and is similar to the structural composition of ordinary liquid water.

Hydrogen bonds with a relatively long lifetime (τ_{life}) of more than 2 ns are identified in the figure by bright blue lines. (For comparison, the average lifetime of hydrogen bonds in liquid water is about 1 ps at $T = 300$ K and 180 ps at 230 K.) In the quiescent stage, these 'long-lasting' hydrogen bonds appear occasionally and randomly at various locations (Fig. 2a). More than 90% of water molecules forming these 'long-lasting' bonds are mostly four-coordinated and their average potential energy is lower than that of other water molecules by more than 2 kJ mol^{-1}.

At $t \approx 256$ ns, a polyhedral structure composed of long-lasting hydrogen bonds forms spontaneously (see the circled region in Fig. 2b). This polyhedron changes its position and shape by altering hydrogen bonds with surrounding water molecules, grows slowly and finally 'anchors' at the position it occupies at $t \approx 290$ ns (Fig. 2c). The nucleus then expands rapidly, by transforming its hydrogen-bond network elements into mainly six-membered rings, which percolate through the entire three-dimensional space of the system. At the same time, the system decreases its total potential energy rapidly (the dark-blue line in Fig. 1). At the end of this period of rapid growth, a 'stacked honeycomb' structure, consisting of six-membered rings, is established throughout most of the system (Fig. 2d).

The number of six-member rings (N_{6R}) fluctuates but never increases significantly before this period of fast growth occurs. We also monitored the so-called Q_6 parameter[15], a commonly used and highly sensitive index for orientational order, which in our system indicates whether or not the relative orientations of hydrogen bonds at individual water sites are coherently ordered. This parameter rises only once the fast growth stage has started, indicating that neither N_{6R} nor Q_6 are order parameters suitable for describing the entire freezing process. During the final freezing stage ($t > 320$ ns), the system undergoes a very slow completion process that involves
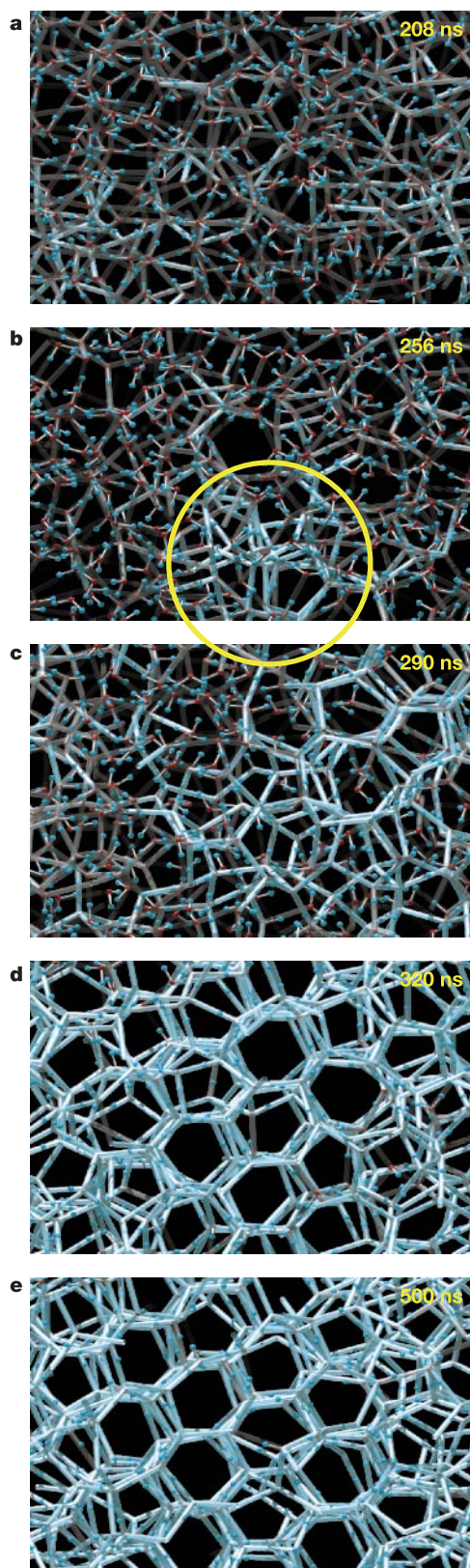
Figure 2 The hydrogen bond network structure of water at a given time in inherent structures. **a**, At time $t = 208$ ns; **b**, at $t = 256$ ns; **c**, at $t = 290$ ns; **d**, at $t = 320$ ns; and **e**, at $t = 500$ ns. Lines indicate hydrogen bonds among water molecules, and the intermolecular bonds of water participating in such hydrogen bonds. Bright blue lines indicate 'long-lasting' hydrogen bonds, which have persisted longer than a specified threshold value before a given time t. The brightest blue lines are those with a lifetime longer than 2 ns ($\tau_{life} > 2$ ns). An initial nucleus is formed in the region circled in **b**.

gradual formation of a perfect honeycomb structure (Fig. 2e) and a concomitant decrease of the potential energy (the purple line in Fig. 1).

Figure 3 illustrates the number of long-lasting hydrogen bonds ($\tau_{life} > 2$ ns) as a function of time. This number changes intermittently in the quiescent period, fluctuates in the initial nucleation period and then rapidly increases after that. During the quiescent period, most of the long-lasting bonds appear intermittently, reminiscent of the intermittent collective motion of water molecules that occurs as a result of extensive hydrogen-bond network rearrangement dynamics of liquid-state water[4–6,16]. A Fourier transform of the fluctuation of the number of long-lasting hydrogen bonds during the quiescent period indeed yields a $1/f$-type power spectrum with the same slope as the structural fluctuation associated with collective motions[17–19]. Such intermittent dynamics is a characteristic of so-called frustrated systems[20,21], such as liquid water.

Although the long-lasting hydrogen bonds are relatively stable, they are randomly scattered and therefore usually unable to form a large stable structure; during the quiescent period, even the long-lasting bonds thus dissipate rapidly again after formation. However, at $t \approx 256$ ns several long-lasting bonds appear by chance in the same location, where they form a polyhedral structure (see Fig. 4) which evolves into a stable initial ice nucleus. The observation that the initial ice nucleus forms by chance as a result of random hydrogen-bond network rearrangement dynamics implies that the length of the quiescent period is randomly distributed.

Using a simple lattice model that captures the tetrahedral hydrogen-bond structure at individual water sites[22,23] to simulate water freezing, we obtained many freezing trajectories. The length of the quiescent periods obtained with this model has a Poisson distribution; that is, the duration of this period is indeed randomly distributed. Similarly, MD calculations for a small system of only 64 water molecules indicated that the length of the quiescent period preceding freezing is apparently random. It should be emphasized, however, that the initial nucleus formation is not an entirely random process; that is, the initial nucleus is created as a result of
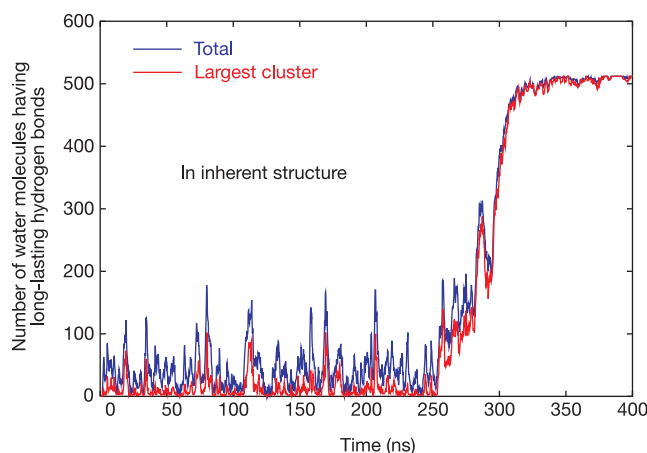

Figure 3 Number of water molecules having long-lasting hydrogen bonds ($\tau_{life} > 2$ ns) and the size of the largest cluster in inherent structures. The number of water molecules having 'long-lasting' hydrogen bonds is indicated by a dark-blue line. See Methods and Fig. 2 legend for the definition of 'long-lasting' hydrogen bonds. The red line indicates the number of water molecules belonging to the largest cluster. A cluster here is defined as a group of water molecules connected by long-lasting hydrogen bonds. We note that the number fluctuates intermittently in the quiescent period ($t = 0$–256 ns), for example, at $t = 20$, 35, 70, 80, 110, 160, 170 and 207 ns. A Fourier transform of this number fluctuation during the quiescent period yields a $1/f$ type power spectrum.

intermittent dynamics (strongly correlated molecular motions), with randomness arising only owing to the need for localization of 'long-lasting' hydrogen bonds.

Figure 4 illustrates how the shape (asphericity) of the nucleus changes during the freezing process when the potential energy slowly decreases ($t = 256-290$ ns in the present trajectory). The initial nucleus formed at $t = 256$ ns is a polyhedron that contains different ring types, does not belong to any well-classified ice or water structure and slightly extends in space. At $t = 260$ ns, it rapidly changes to a more compact form (that is, one of small asphericity) while decreasing in cluster size. This nucleus then grows slowly while changing its shape extensively. At $t = 270$ ns, the nucleus again adopts a very compact structure, but is now relatively large; it may in fact be beyond the size of the 'critical nucleus' that plays a central role in homogeneous nucleation theory[14]. Restarting from the instantaneous configurations along the present trajectory, we performed more than 100 trajectory calculations using different initial molecular velocities. Trajectories restarting from this nucleus structure at $t = 270$ ns indeed crystallize quickly, similar to the

behaviour seen in the original trajectory shown in Fig. 1. In contrast, only a very small portion, 9%, of the trajectories restarting from the configurations reached during the period $t = 240-256$ ns start to crystallize within 100 ns. The percentage of the trajectories successfully crystallized increases with the restarting time; 29% for those restarting from the configurations during $t = 256-265$ ns and 60% for those during $t = 265-270$ ns. These observations imply that the formation of a nucleus with the critical or minimum size for crystallization occurs during this period, $t = 256-270$ ns. The growth of the nucleus increases around $t = 282$ ns and becomes very rapid after $t = 290$ ns (see Fig. 3). During the period when the initial nucleus is formed ($t = 256-270$ ns) the inherent structure analysis, finding the nearest local potential energy minima along the trajectory (see Methods), yields a very rugged potential energy landscape (see Fig. 1 inset). The average potential energy of individual water molecules constituting the initial nucleus is $4-6$ kJ mol^{-1} ($4-6$%) lower than that of other water molecules, with the exact value depending on the shape of the nucleus (the average potential energy is lower for more compact forms).

In the quiescent period, many long-lasting hydrogen-bond clusters appear intermittently, but their shape is much less compact than that of the cluster formed at $t = 256$ ns. For example, the polyhedron at $t = 207$ ns is larger but also significantly more extended than the polyhedron seen at $t = 256$ ns (see the inset of Fig. 4) and thus rapidly disappears.

The size of the critical nucleus must sensitively depend on its shape and on the size of system employed in MD. A larger system with 4,096 water molecules also yields extensive changes of nucleus shape (asphericity) during the period of initial nucleus formation, before entering the period of rapid growth. For much larger systems, the overall potential energy change associated with the formation of the initial nucleus and its subsequent rapid growth is fairly smooth, unlike the distinct changes seen in Fig. 1 for the system of 512 water molecules. The size of this system might be too small to deal with the detailed mechanism underlying the rapid growth.

Our MD trajectories under constant-temperature and constant-volume conditions have elucidated the molecular-level mechanism involved in water freezing, but the calculations do not account for important factors that might significantly affect the nucleation rate. For example, liquid water at low temperature exhibits large-scale density fluctuations[24,25], which have been interpreted to mean that there are regions of low-density liquid phase that facilitate initial nucleus formation. These low-density regions induce 'wetting' of the nucleus—that is, a matching of the density and hence the lattice constant of the surrounding liquid with that of the nucleus—thus facilitating the formation of hydrogen bonds between the two states and hence rapid crystal growth. (This effect is partly included in the present calculations by using a slightly reduced water density of 0.96 g cm^{-3}.) It will be of interest to determine whether the crystallization rate diminishes if the large scale density fluctuations in water are reduced by some means[2], and whether such a reduction would make it possible to obtain amorphous ice instead of crystalline ice under ambient conditions. The kinetic energy released by local crystallization might provide the excess energy needed to cross over the barriers on the rugged potential energy surface. To investigate these effects, MD simulations under constant pressure and with a detailed description of local temperature variations should be performed for very large systems. Finally, in order to obtain a more quantitative molecular-level description of nucleation, a free energy surface along an 'ordering parameter' (for example, a characteristic tetrahedral ordering parameter) needs to be constructed and evaluated. Such results would allow an assessment of the validity of the nucleation rate theory derived from thermodynamics and help to identify the intrinsic dynamical effects that control the water-freezing process. □
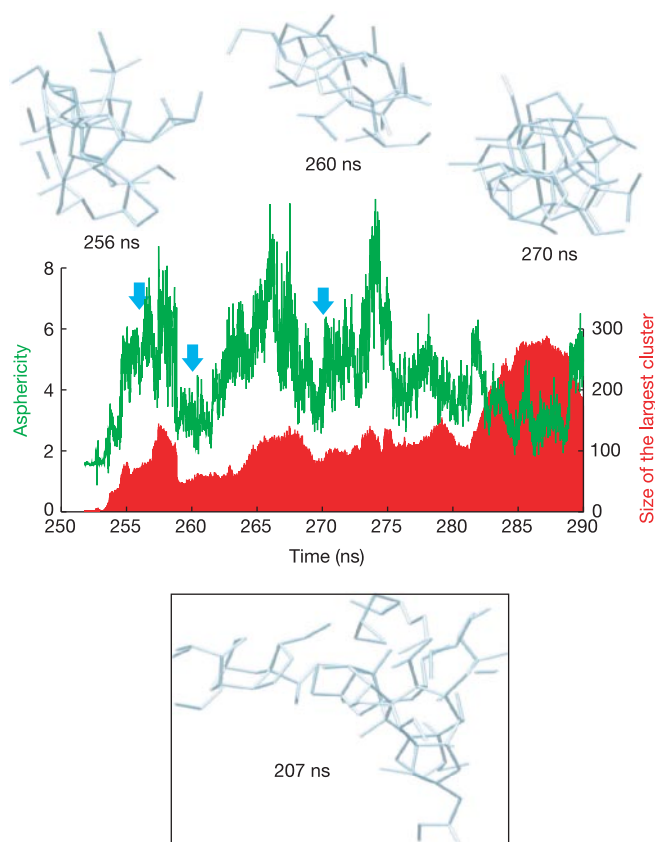

Figure 4 Asphericity and size of the largest cluster. Asphericity (green line) is calculated at 10-ps intervals for inherent structures. A cluster is defined as a group of water molecules connected by long-lasting hydrogen bonds. We assign Voronoi polyhedra to individual water molecules belonging to this nucleus. The shape of the nucleus is represented by a polyhedron which consists of these Voronoi polyhedra. Asphericity of the nucleus is defined as the cube of the surface area divided by the square of the volume of this polyhedron, renormalized to yield the asphericity of a sphere to be 1. Asphericity increases as the shape deviates from the sphere; for example, it is 1.9 for a cube. The size of the largest cluster (red bar lines) is defined as the number of water molecules belonging to the nucleus. The structures of the largest cluster (nucleus) for $t = 256$, 260 and 270 ns are also shown (blue arrows from left to right), as well as that at $t = 207$ ns (whose cluster size is 100) in the inset.

Methods

Molecular dynamics (MD) calculations are performed for 512 molecules contained in a cubic box with the periodic boundary. A time step in MD is 1 fs (femtosecond; 10^{-15} s). In the present study, a constant-volume ($0.96\,\mathrm{g\,cm}^{-3}$) and constant-temperature MD is employed. The Nose–Hoover method is used to control the temperature. An empirical water model, TIP4P, is used to describe the water–water molecular interaction. Intermolecular interaction is cut off smoothly as in previous studies[5,6,16]. MD trajectories are performed for different temperatures, but so far only one at 230 K undergoes the crystallization for 512 water molecules. We have performed 6 trajectory calculations of the order of microseconds, but only the one that successfully crystallized is presented in this work. An individual trajectory calculation of this size system takes several months in a supercomputer. One trajectory with 220 K is found to stop in a partially crystallized structure. Those with higher temperatures have never resulted in freezing. MD calculations were also performed for various size systems containing 64, 96, 216, and 4,096 water molecules. For 4,096 water molecules, a freezing process is also attained at 230 K. Constant-pressure and constant-temperature trajectories have also been performed for various sizes of systems but crystallization has so far been achieved only for a very small system (64 water molecules). These constant-pressure, constant-temperature trajectories show that large density fluctuations are always associated with the freezing process. An inherent structure analysis[26] is performed by applying a local quenching method; the inherent structures are local minima of the potential wells sequentially visited by the system in a trajectory. In the inherent structure description, vibrational motions are thus removed, revealing the fundamental hydrogen-bond structure changes along the trajectory[4–6,26].

1. Swope, W. C. & Andersen, H. C. 10^6 particle molecular-dynamics study of homogeneous nucleation of crystals in a supercooled atomic liquid. *Phys. Rev. B* **41**, 7042–7054 (1990).
2. Wolde, P. R. & Frenkel, D. Enhancement of protein crystal nucleation by critical density fluctuation. *Science* **277**, 1975–1978 (1997).
3. Ball, K. D. *et al*. From topographies to dynamics on multidimensional potential energy surfaces of atomic clusters. *Science* **271**, 963–966 (1996).
4. Ohmine, I. & Saito, S. Water dynamics: fluctuation, relaxation, and chemical reactions in hydrogen bond network rearrangement. *Acc. Chem. Res.* **32**, 741–749 (1999).
5. Ohmine, I. Liquid water dynamics; collective motions, fluctuation and relaxation. *J. Phys. Chem.* **99**, 6767–6776 (1995).
6. Ohmine, I. & Tanaka, H. Fluctuation, relaxation and hydration in liquid water. Hydrogen-bond rearrangement dynamics. *Chem. Rev.* **93**, 2545–2566 (1993).
7. Svishchev, I. M. & Kusalik, P. G. Electrofreezing of liquid water: A microscopic perspective. *J. Am. Chem. Soc.* **118**, 649–654 (1996).
8. Nada, N. & Furukawa, Y. Anisotropic growth kinetics of ice crystals from water studied by molecular dynamics simulation. *J. Cryst. Growth* **169**, 587–597 (1996).
9. Koga, K., Tanaka, H. & Zeng, X. C. First-order transition in confined water between high-density liquid and low-density amorphous phases. *Nature* **408**, 564–567 (2000).
10. Onuchic, J. N., Luthey-Schulten, Z. & Wolynes, P. G. Theory of protein folding: the energy landscape perspective. *Annu. Rev. Phys. Chem.* **48**, 545–600 (1997).
11. Dobson, C. M. & Karplus, M. The fundamentals of protein folding: bringing together theory and experiment. *Curr. Opin. Struct. Biol.* **9**, 92–101 (1999).
12. Kramer, B. *et al*. Homogeneous nucleation rates of supercooled water measured in single levitated microdroplets. *J. Chem. Phys.* **111**, 6521–6527 (1999).
13. Bartell, L. S. Nucleation rates in freezing and solid-state transitions. *J. Phys. Chem.* **99**, 1080–1087 (1995).
14. Abraham, F. F. *Homogeneous Nucleation Theory* (Academic, New York, 1974).
15. Steinhardt, P. J., Nelson, D. R. & Ronchetti, M. Bond-orientational order in liquids and glasses. *Phys. Rev. B* **28**, 784–805 (1983).
16. Ohmine, I., Tanaka, H. & Wolynes, P. G. Large local energy fluctuation in water. *J. Chem. Phys.* **89**, 5852–5860 (1988).
17. Sasai, M., Ramaswamy, R. & Ohmine, I. Long time fluctuation of liquid water. *J. Chem. Phys.* **96**, 3045–3053 (1992).
18. Walrafen, G. E., Hokmabadi, M. S., Yang, W.-H., Chu, Y. C. & Monosmith, B. Collision-induced Raman scattering from water and aqueous solutions. *J. Phys. Chem.* **93**, 2909–2917 (1989).
19. Saito, S. & Ohmine, I. Translational and orientational dynamics of a water cluster $(H_2O)_{108}$ and liquid water. *J. Chem. Phys.* **102**, 3566–3576 (1995).
20. Metzler, R. & Klafter, J. The random walk's guide to anomalous diffusion: a fractional dynamics approach. *Phys. Rep.* **339**, 1–77 (2000).
21. Weissman, M. B. 1/f noise and other slow, non-exponential kinetics in condensed matter. *Rev. Mod. Phys.* **60**, 537–571 (1988).
22. Sasai, M. Instabilities of hydrogen bond network in liquid water. *J. Chem. Phys.* **93**, 7329–7341 (1990).
23. Matsumoto, M. & Ohmine, I. New approach to dynamics of hydrogen bond network in liquid water. *J. Chem. Phys.* **104**, 2705–2712 (1996).
24. Mishima, O. & Stanley, H. E. The relationship between liquid, supercooled and glassy water. *Nature* **396**, 329–335 (1998).
25. Sastry, S., Debenedetti, P. G., Sciortino, F. & Stanley, H. E. Singularity-free interpretation of the thermodynamics of supercooled water. *Phys. Rev. E* **53**, 6144–6154 (1996).
26. Stillinger, F. H. & Weber, T. A. Packing structures and transitions in liquids and solids. *Science* **225**, 983–989 (1984).

Competing interests statement

The authors declare that they have no competing financial interests.

....

Active fluidization of polymer networks through molecular motors

D. Humphrey*, C. Duggan*, D. Saha*, D. Smith* & J. Käs*†‡§

* *Center for Nonlinear Dynamics,* † *Institute for Cellular and Molecular Biology, and* ‡ *Texas Materials Institute, and* § *Center for Nano and Molecular Science, University of Texas at Austin, Texas 78712, USA*

....

Entangled polymer solutions and melts exhibit elastic, solid-like resistance to quick deformations and a viscous, fluid-like response to slow deformations. This viscoelastic behaviour reflects the dynamics of individual polymer chains driven by brownian motion[1]: since individual chains can only move in a snake-like fashion through the mesh of surrounding polymer molecules, their diffusive transport, described by reptation[2–4], is so slow that the relaxation of suddenly imposed stress is delayed. Entangled polymer solutions and melts therefore elastically resist deforming motions that occur faster than the stress relaxation time. Here we show that the protein myosin II permits active control over the viscoelastic behaviour of actin filament solutions. We find that when each actin filament in a polymerized actin solution interacts with at least one myosin minifilament, the stress relaxation time of the polymer solution is significantly shortened. We attribute this effect to myosin's action as a 'molecular motor', which allows it to interact with randomly oriented actin filaments and push them through the solution, thus enhancing longitudinal filament motion. By superseding reptation with sliding motion, the molecular motors thus overcome a fundamental principle of complex fluids: that only depolymerization makes an entangled, isotropic polymer solution fluid for quick deformations.

Actin and myosin II are the key elements of the contractile machinery in muscle cells. Myosin's motor domains, or 'heads', bind actin filaments (F-actin) and exploit adenosine triphosphate (ATP) hydrolysis to generate a force to move along polar actin filaments towards the positive end. *In vitro* and in non-muscle cells, myosin II proteins assemble into multimeric bipolar structures with motor domains on both ends[6–9] known as minifilaments. Several of the myosin heads at the end of these minifilaments attach to actin filaments. When ADP (adenosine diphosphate) is substituted for ATP in solution, the minifilaments crosslink F-actin via the inactive heads. In this case the actin–myosin sample assumes a solid, gelatin-like consistency (Fig. 1a). In the presence of ATP, myosin is active and the sample behaves like a fluid (Fig. 1a). The myosin heads push the actin filaments and collectively induce sliding of filaments in the presence of ATP[10] (Fig. 1b). Similar to two-dimensional motility assays[11] in which F-actin moves on myosin heads adsorbed to a cover slide, filaments are unidirectionally pushed by myosin towards their negative ends. The sliding filaments are oriented at a variety of angles with respect to each other.

By inducing active filament sliding instead of thermally driven